J Nanopart Res (2012) 14:896
DOI 10.1007/s11051-012-0896-3

RESEARCH PAPER

Cluster models of aqueous Na^+ and Cl^- in sea water/ice

R. Michelsen · R. Walker · D. Shillady

Received: 28 November 2011 / Accepted: 2 May 2012

Abstract In this article, we present finite cluster models of aqueous solutes [$NaCl(H_2O)_{10}$, $NaCl(H_2O)_5$, and $(H_2O)_6$] in terms of molecular geometry and vibrational spectra for interpretation of experimental infrared spectra of NaCl brine solutions. The quantum chemistry program GAMESS is used to optimize the model clusters to a local minimum energy gradient of less than 5.0d-6 hartrees/bohr with B3LYP in a gaussian basis of 6-31G(d,p). Harmonic frequencies are computed for comparison with the infrared spectra measured by attenuated total reflection of a temperature-controlled Ge plate under a layer of cold brine solution. The motivation for this research is to understand the mechanism by which freezing seawater excludes halide ions (mainly Cl^-) and why the O–H stretching region of the spectra changes with temperature. Frost flowers, sea ice, and snow in marine environments contain concentrated halides in liquid brine at their surfaces which lead to catalytic destruction of low-altitude ozone in the polar regions of the Earth.

Keywords Sea ice · Frost flowers · $NaCl(H_2O)_5$ · Brine · Vibrational spectra · Modeling and simulation · Atomic clusters

Introduction

Chemists are usually aware that salts of alkali metals and halides readily dissociate in water. The Debye–Hückel (Debye and Hückel 1923) theory of dilute solutions has been developed to understand the lowered "activity" of solvated ions, in essence, the screening of the ions by at least one layer of solvent molecules. Solutions of 1 mol of NaCl/L of solution (1 M) or less have a ratio of more than 50:1 water molecules per NaCl unit, and we might expect individual clusters like $Na^+(H_2O)_6$ and $Cl^-(H_2O)_6$ to exist. This is supported by solution conductance data (Barrow 1988) which can be extrapolated to "infinite dilution" values for individual solvated ions. Such solvated ions can be modeled under C_{2V} symmetry with Restricted Hartree–Fock (RHF) calculations (Roothaan 1951) in a 6-31G(d) basis as shown in Fig. 1. Higher concentration (saturated) salt solutions have been studied at room temperature (26.5 °C) (Max and Chapados 1999), with the limit having been found to be five water molecules for NaCl (5.13 M), KCl, and other alkali metal salts.

This article is part of the topical collection on nanomaterials in energy, health and environment

R. Michelsen · R. Walker
Department of Chemistry, Randolph-Macon College, Ashland, VA, USA

D. Shillady (✉)
Department of Chemistry, Virginia Commonwealth University, Richmond, VA, USA
e-mail: quantummechanicsllc@msn.com

Published online: 18 September 2012

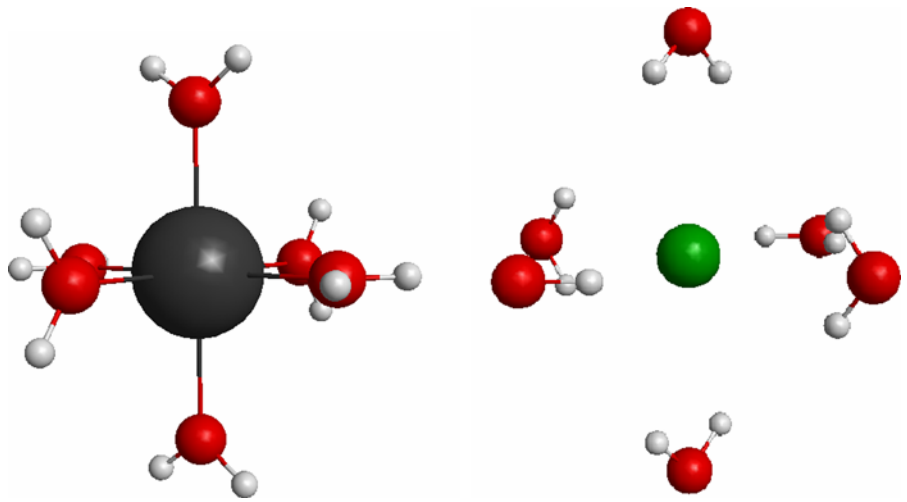

Fig. 1 The RHF 6-31G(d) optimized C_{2V} ion clusters for $Na^{+}(H_2O)_6$ on the *left*, and $Cl^{-}(H_2O)_6$ on the *right*. The drawings are not to scale, but the chloride structure is slightly larger

Although solutes will depress the freezing point of an aqueous solution, the water will still freeze at the lower temperature. When the water freezes, the concentration of the NaCl in the unfrozen brine will increase until it reaches some limiting number of water molecules that can keep it in solution. The application of interest here is the exclusion of halide ions from sea ice resulting in salt concentrations much higher than 1 M.

Initial computations for $Na^{+}(H_2O)_6$ and $Cl^{-}(H_2O)_6$ did not lead to satisfactory explanations for the observed temperature shift of the O–H stretching region of NaCl brine/ice. Other studies (Max and Chapados 2001) claim that aqueous ion pairs such as $NaCl(H_2O)_5$ and $KCl(H_2O)_5$ persist in solution and exist especially at higher salt concentrations. The large volume of literature on rapid precipitation of insoluble materials from (dilute) aqueous salt solutions (Hogness and Johnson 1954) argues for the existence of independent solvated ions or at least easy dissociation of ion pairs in solution. Even so, the spectroscopic evidence (Max and Chapados 1999, 2001) strongly supports the empirical formulas for small finite clusters of ion pairs in solution solvated by only five water molecules, especially at concentrations as high as 5.13 M (26.5 °C).

In this study, we apply the ground-breaking concept of the use of finite molecular nano-clusters to model bulk phenomena, first brought to our attention by Puru Jena in 1982. Physicists are usually aware that crystalline solid lattices obey a constraint of infinite repetition. Thus, it was a major innovation when finite cluster models of solids appeared at the first ISCAN Meeting (Shillady et al. 1982). Here, it seems appropriate to extend the finite cluster concept to a problem involving highly concentrated solutions using finite nano-molecular species. Even though liquids are more dynamic than solids, molecular modeling can lend insight into behavior at the atomic level.

Recently, there has been interest in molecular dynamic studies of brine solutions (Jungwirth and Tobias 2001) which show that halide ions tend to be at the surface of the liquid. If halides are close to the surface on polar sea ice they may act as a catalyst after reaction to form species such as BrCl which destroy ozone at low altitude over the polar ice caps (Foster et al. 2001). Mercury (Hg) vapors may also be oxidized to Hg^{+2} by halides (Lu et al. 2001) because of the high salinity of frost flowers formed on sea ice (Douglas et al. 2005). In addition, frost flowers (Alvarez-Aviles et al. 2008), several centimeters or higher as observed on sea ice, offer a greatly increased area of catalytic surface for excluded Cl^{-} and Br^{-} ion sites where reactive gas-phase species can form. Frost flowers can be created by sea water freezing (Douglas et al. 2005) in an air environment at least 15 °C colder. They can then act as wicks for seawater where freezing can increase the halide concentration. The salinity of the total volume of frost flowers has been documented at about three times higher than that of seawater

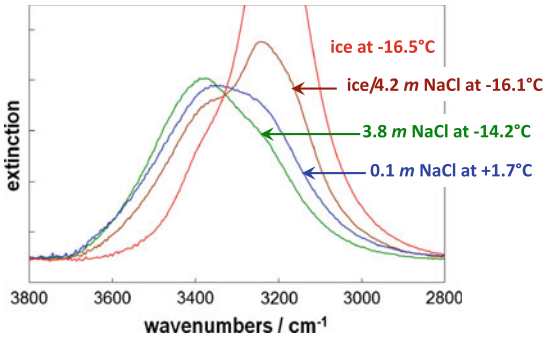

Fig. 2 Experimental spectra of 0.1 M NaCl brine frozen to −17 °C and gradually warmed. Melted brine first noted at −16.1 °C. The spectrum of pure ice is shown for comparison

(Douglas et al. 2005). The concentrations of NaCl and KCl in seawater are relatively low, with a combined Cl^- concentration of roughly 0.55 M. However, we consider the possibility that freezing sea water can increase the concentration to more than 4 M on the catalytic surface of the fern-like frost flowers as water freezes leaving more concentrated brine. We study both the tendency for chloride ions to be at the liquid surface and the change in NaCl concentration as the freezing temperature is attained for sea ice.

The experimental data we have obtained for the concentrated NaCl solutions show a small blue shift in the O–H stretching region of the cold, concentrated brine spectra relative to both the warmer, more dilute solution, and to pure water ice as shown in Fig. 2. This effect is small in comparison to the very intense peak at about 3,180.1/cm observed here due to freezing of a 0.1 M NaCl solution into ice **I**. Of most interest is the blue shoulder in the spectrum at −16.1 °C where there is the highest concentration of NaCl in the brine at near-equilibrium with melting ice. Thus, we have included modeling of cyclic $-(H_2O)_6$ in the chair conformation which is the primary repeating group in the unit cell of ice **I** (Davidson and Morokuma 1984). We postulate that the spectroscopic features to the blue of the main ice peak are due to cluster species such as $NaCl(H_2O)_{10}$ and $NaCl(H_2O)_5$ in the brine.

Method

The brine spectra were collected using a temperature-controlled attenuated total reflectance (ATR) cell in a Thermo Nicolet Fourier Transform Infrared spectrometer as shown. Many scans were obtained for pure

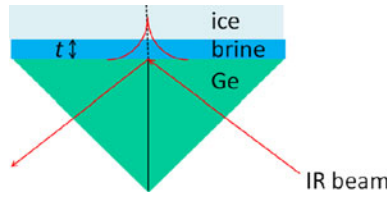

Fig. 3 A cartoon of the ATR experiment showing an ice film with an interfacial liquid brine layer on the Ge crystal with a thickness of *t*. The IR beam measures mainly the brine spectrum in a layer that is <1 μ (10^{-4} cm) thick

water and various frozen brine solutions over a range of temperatures (−17 to 25 °C). Frozen films were observed to have an interfacial layer of liquid brine, as shown in Fig. 3. In this study, only NaCl was studied as obtained from Sigma Aldrich (>99.0 %) dissolved in ACS reagent grade water. The spectra in Fig. 2 were obtained by freezing an initial 0.1 M solution of NaCl at −17 °C and slowly warming the sample (10–15 min/degree). It was assumed that the ice film and the liquid brine were in equilibrium. Thus, using the formula fitted to molal freezing point depression given in the *Handbook of Chemistry and Physics* (Haynes 2012), we can estimate the effective concentration of the brine by solving the equation for the molality (m, gram moles/1,000 gm of H_2O). At −16.1 °C using $\Delta T(^\circ\mathrm{C.}) = -0.1874m^2 - 3.0227m - 0.123$, we find $m = 4.20515 \cong 4.2$. It is preferable to use molality (m) rather than molarity (M) because molality is independent of the density of the solution. The experimental limit for ice formation in the spectra of Fig. 2 indicates our concentration is slightly less than the room temperature concentration used by Max and Chapados.

The geometries of the finite cluster species were optimized to better than 5.0d-6 hartrees/bohr (1.0d-7 some cases) using the 2008 Version 11 of the GAMESS program (Gordon and Schmidt 2005) on a personal computer running on Red Hat LINUX V under the Centos-04 V4.6 operating system. A number of initial structures were optimized using the RHF–SCF method (Roothaan 1951) such as $Na^+(H_2O)_6$, $Cl^-(H_2O)_6$, $NaCl(H_2O)_{11}(C_{2V})$, $NaCl(H_2O)_{13}(C_{2V})$, and $NaCl(H_2O)_{24}$. In all cases it was evident that the average distance of H_2O from Cl^- was slightly larger than the Na^+-OH_2 distance. In this article, we only present the results for $NaCl(H_2O)_5$, $NaCl(H_2O)_{10}$, and $(H_2O)_6$ which seem to best fit the experimental facts (Table 1).

Table 1 Computational results for selected clusters

Cluster	Energy (Hartree)	Dipole (Debye)	R_{NaCl} (ang.)
NaCl-RHF**	−621.3996181773	9.529541	2.3970362
NaCl-MP2**(fc)	−621.5343677135	9.157499	2.3931564
NaCl-BLYP**	−622.5261586055	8.291397	2.3892415
NaCl-B3LYP*	−622.4526461328	8.657008	2.3770143
$NaCl(H_2O)_5$-RHF**	−1001.5852744430	4.526342	2.6891961
$NaCl(H_2O)_5$-MP2**(fc)	−1002.6764523386	3.924395	2.6688149
$NaCl(H_2O)_5$-BLYP**	−1004.6318662779	3.784873	2.7726373
$NaCl(H_2O)_5$-BLYP*	−1004.6832932854	3.616036	2.7821160
$NaCl(H_2O)_5$-B3LYP*	−1004.5262235236	3.804715	2.7472803
$NaCl(H_2O)_{10}$-RHF**	−1381.7289979455	5.071972	4.2677457
$NaCl(H_2O)_{10}$-MP2**(fc)	−1383.7841083757	4.683000	4.1775910
$NaCl(H_2O)_{10}$-BLYP*	−1386.8038830587	3.954168	4.0259432
$NaCl(H_2O)_{10}$-B3LYP*	−1386.5633869036	4.047412	4.0037374

fc frozen core
* 6-31G(d,p)
** 6-31G(d)

Infrared absorption was explored using MP2 (Binkley and Pople 1975) calculation of the vibrational frequencies using a small 6-31G(d) basis set without 2p orbitals on the H atoms. The MP2 calculations used the frozen core (fc) approximation so that correlation energy was only computed for the valence shell orbitals. These calculations indicated that $NaCl(H_2O)_5$ is central to this study, and so geometric configurations were also optimized using the BLYP (Becke 1988; Lee et al. 1988) and B3LYP (Becke 1988, 1993a, 1996) functionals to a gradient threshold of 5.0d-6 hartrees/bohr with a better basis of 6-31G(d,p) to see if adding 2p orbitals on the H atoms changed the geometry or frequencies. No significant geometric difference was observed with the 6-31G(d,p) results, although adding H-2p orbitals lowered the BLYP energy of $NaCl(H_2O)_5$ by roughly 0.051 hartrees.

The 6-31G(d) basis was used for the initial frequency calculations because the Scott–Radom's correction factor (Scott and Radom 1996) for BLYP 6-31G(d) frequencies found to be equal to 0.9945 is very close to 1. That facilitated making peak assignments, but the basis did not include 2p orbitals for hydrogen bonding. Geometric configurations were first optimized roughly using the RHF method and then further optimized using both the MP2 (Binkley and Pople 1975) and BLYP form of correlation calculation. Although MP2 calculations were shown to be superior to over 40 density functionals available in 2005 for weak interactions by Truhlar (Zhao and Truhlar 2005), we also used the B3LYP functional (Becke 1988, 1993b, 1996) with a larger 6-31G(d,p) basis. B3LYP results have been shown to be close to very accurate coupled cluster calculations (Su et al. 1999). However, the B3LYP frequency correction factor is slightly worse at 0.9613 (Foresman and Frisch 1996) for 6-31G(d) compared to the BLYP factor of 0.9945, while the MP2 factor is 0.9434. We were unable to locate a separate scaling factor for the 6-31G(d,p) basis, but the same factor has been used successfully for both 6-31G(d) and 6-31G(d,p) (Callahan et al. 2007).

The MP2 results converged cleanly to 2.0d-7 hartrees/bohr and produced a short Na–Cl distance of 2.67 angstroms. The bond analysis showed that the Na–Cl interaction is an ion pair, not a bond, since the "bond order" was 0.029 in the converged MP2 results compared to the bond order of 0.789 for the NaCl molecule using B3LYP with a 6-31G(d,p) basis. In the case of $NaCl(H_2O)_{10}$ the longer Na–Cl bond length (greater than 4 angstroms) led to an unreported bond order less than 0.05, and the dipole moment increased slightly, indicating an ion-pair, not a chemical bond.

The simulated infrared spectra were calculated using the peak height from the GAMESS dipole intensity of the harmonic vibrational modes with a gaussian band shape of 40.1/cm width at (1/e) height. This band width is smaller than the broad experimental band width, but it permits artificial resolution and analysis of which bands are contributing to the experimental spectrum at various (1/cm) values. The computed dipole intensities were draped with the gaussian band shape using a small f77 program as has

been previously shown to be useful (Esperdy and Shillady 2001).

Results

The spectral change with temperature is a small blue shift of the NaCl brine relative to ice. The ATR spectrometer measures mainly the thin layer of brine solution under the ice layer in equilibrium with the ice as it slowly melts. In order to provide a graphic display, a small unit of ice **I** was optimized as three rings of cyclic $(H_2O)_6$ in the chair conformation shown in Fig. 4. The block of 18 water molecules converged easily to a tight RHF minimum of 1.0d-7 hartree/bohr with a 4-31G basis. The chair form shown stacked as parallel rings in the RHF 4-31G optimization is similar to a previous structure (Davidson and Morokuma 1984) which showed alternating chair forms. Using the finite cluster concept, we chose to model a component of the brine in equilibrium with ice as $(H_2O)_6$.

The B3LYP optimized structure for a single ring shown in Fig. 5 is more flattened, with the distance between the O atoms being about 2.8 angstroms. The chair conformation of cyclohexane $(CH_2)_6$ is based on the tetrahedral angle of CH_4 of 109.5° while the HOH angle in water is 104.5° (Eisenberg and Kauzmann 1969), and so we find a chair conformation more nearly planar for $(H_2O)_6$. Almost the entire IR intensity near 3,200.1/cm is due to two normal modes which allow a synchronous movement of the H atoms along the hydrogen bonds around the ring, and so we believe that we have captured most of the O–H band intensity without including the interaction between two or more $(H_2O)_6$ clusters. There is probably some lone $(H_2O)_6$ in the solution just coming off the ice crystals in the slow warming sequence of our data. In Fig. 6, the intensity of these modes dominates the simulated spectrum of the NaCl brine in agreement with the experimental brine spectra at −16.1 °C as shown in Fig. 2.

In this study, we are only interested in the O–H stretching region of the spectrum near 3,200.1/cm. The spectra for $NaCl(H_2O)_5$ and $NaCl(H_2O)_{10}$ were computed using MP2, BLYP, and B3LYP calculations but the B3LYP 6-31G(d,p) spectra are shown as they are likely to be the most accurate. The smaller cluster of

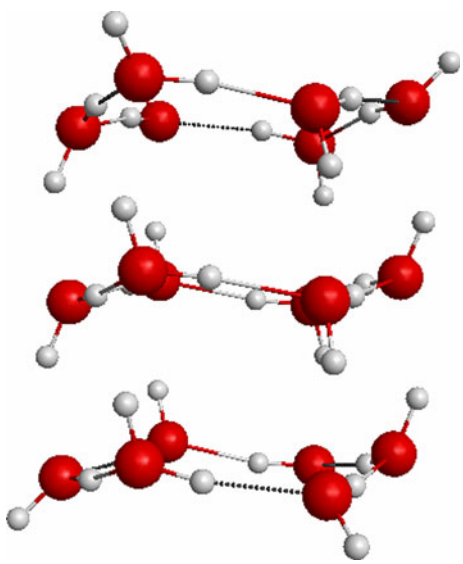

Fig. 4 A small section of ice **I** optimized to a gradient of 1.0d-7 hartree/bohr using RHF with a 4-31G basis

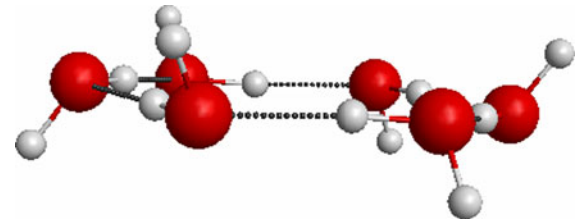

Fig. 5 Chair form of $(H_2O)_6$ optimized using B3LYP with a 6-31G(d,p) basis. The structure is nearly planar due to the smaller HOH angle of 104.5° compared to the CCC angle of 109.5° in cyclohexane

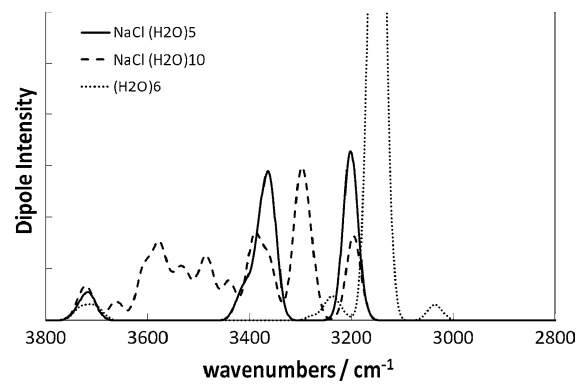

Fig. 6 Combined B3LYP 6-31G(d,p) spectral simulation scaled by 0.9613 for $NaCl(H_2O)_5$, $NaCl(H_2O)_{10}$, and $(H_2O)_6$ as an explanation/model of the blue shift of NaCl ice/brine just above the melting point

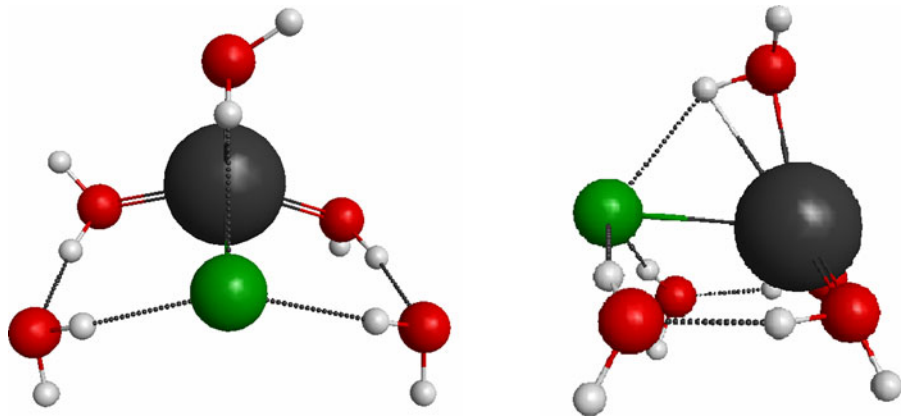

Fig. 7 Two views of the optimized structure for $NaCl(H_2O)_5$ using B3LYP with a 6-31G(d,p) basis set (Max. Grad. = 2.5d-6 hartrees/bohr, RMS Grad. = 9.0d-7). The geometry obtained from RHF, MP2, BLYP(d), and BLYP(d,p) varied only slightly from this structure. The "double bonds" are the way in which MacMolPlt (Bode and Gordon 1998) indicates a short bond length. Hydrogen bonds are shown as dotted lines

$NaCl(H_2O)_5$ has fewer normal modes (45) than $NaCl(H_2O)_{10}$ (90) using the finite cluster concept. The spectra for the $NaCl(H_2O)_5$ cluster yielded a few intense peaks just close to the blue of the strong absorption bands of $(H_2O)_6$. Four of the five water molecules around the NaCl ion pair, as shown in Fig. 7, form a plane of hydrogen bonds which have a very intense absorption due to a synchronous motion of four H atoms. This smaller ring of only four water molecules has a higher resonant frequency than the six-member ring of $(H_2O)_6$, and it produces a strong spike to the blue of the $(H_2O)_6$ peak. However, since $NaCl(H_2O)_5$ has fewer modes relative to bulk water the band intensity falls off further to the blue.

Figure 6 shows a combined simulated spectrum of the melting 4.2 M NaCl brine. The computed spectrum for $NaCl(H_2O)_5$ alone is too narrow to account for the observed blue shift. Thus, we have also calculated the spectrum for $NaCl(H_2O)_{10}$. Our initial guess at a structure was to use the optimized octahedral structures for $Na^+(H_2O)_6$ and $Cl^-(H_2O)_6$. The two octahedral clusters were brought together by removing one water molecule from each cluster along the NaCl bond. A previous optimization was

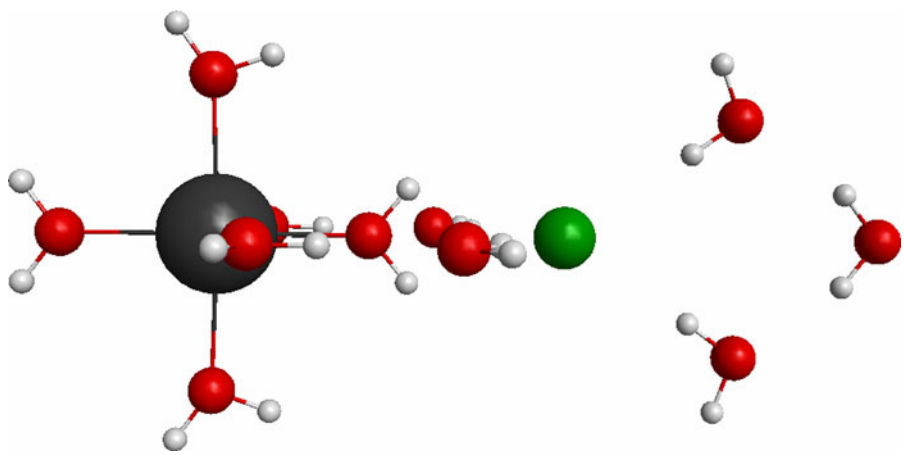

Fig. 8 The RHF C_{2V}-idealized geometry of $NaCl(H_2O)_{11}$ based on the structures of $Na^+(H_2O)_6$ and $Cl^-(H_2O)_6$ using a common water molecule bridge. This structure underwent substantial relaxation when the C_{2v} symmetry constraint was removed along with the H_2O bridge

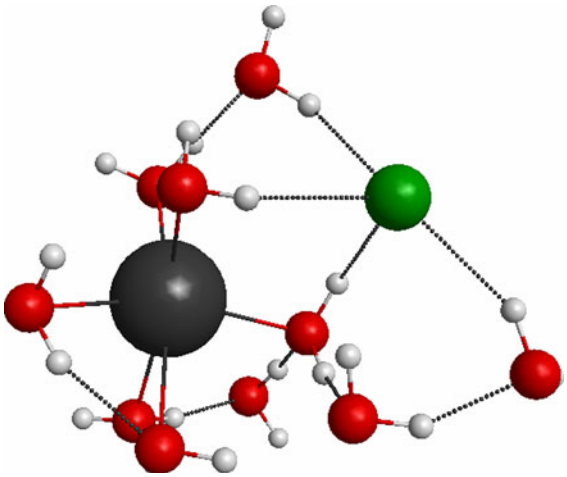

Fig. 9 A B3LYP 6-31G(d,p)-optimized structure for $NaCl(H_2O)_{10}$

successful for $NaCl(H_2O)_{11}$ under C_{2V} constraint with one water molecule acting as a bridge between Na^+ and Cl^- shown in Fig. 8. This suggested a numerical experiment to estimate the relative tendencies of Na^+ and Cl^- to attract water molecules. When the bridging water molecule and the artificial C_{2V} constraint were removed, the structure relaxed to a very different geometry as shown in Fig. 9 as $NaCl(H_2O)_{10}$. The calculated absorption bands are very large in number in the 3,200–3,500.1/cm range and span a larger range because the water molecules are present in several environments. The $NaCl(H_2O)_{10}$ cluster represents a situation in which the ratio of water molecules to NaCl ions is lower than that for independently solvated ions. Thus, in Fig. 6 are presented our best estimates of the combined components leading to the observed experimental brine spectrum.

Although the structure of $NaCl(H_2O)_{10}$ was derived from C_{2V} $[(H_2O)_5Na^+](H_2O)[Cl^-(H_2O)_5]$, the robust energy minimization in GAMESS (Gordon and Schmidt 2005) resulted in a structure where Na^+ is preferentially solvated while the Cl^- is left to bind mainly with the Na^+ ion and seemingly excluded from the water. Note that the Cl^- ion is only held by four weak bonds to hydrogen and ion attraction to whatever residual positive charge there is from the Na^+ ion. This limited example is compatible with the earlier molecular dynamic studies (Jungwirth and Tobias 2001) which predict a preference of halide ions for the surface of a brine. During geometric optimization of $NaCl(H_2O)_{10}$ several local minima were encountered, and so the structure shown in Fig. 9 is probably not unique. However, Fig. 9 shows one accessible geometry in the dynamic motion of the liquid. The most important result of the experiment is that the Na^+ ion attracts water molecules more than the Cl^- ion. In the case of water deficiency, the chloride ion will tend to be expelled from the solution toward some interface.

Because the spectrum of $NaCl(H_2O)_5$ is relatively narrow and sharp, we estimate the presence of this species just before freezing occurs along with other water-deficient clusters similar to $NaCl(H_2O)_{10}$ adding width to the spectrum. Clusters, such as $NaCl(H_2O)_8$ etc., may occur as well in a water-deficient brine but we have chosen to study the vibrational spectrum of $NaCl(H_2O)_{10}$ to include a wider range of water molecules in differing environments near the Na^+Cl^- ion pair.

We have not attempted to fit the experimental spectrum by a factor analysis as has been done by others (Max et al. 2001), but qualitatively the computed spectra of $NaCl(H_2O)_5$ and $NaCl(H_2O)_{10}$ match the observed shoulder on the spectrum shown in Fig. 2 at −16.1 °C and the peak at −14.2 °C sufficiently well so as to support the presence of $NaCl(H_2O)_5$ and other water-deficient solvated ions. Thus, in our interpretation, there may be a number of other water-deficient clusters in the brine at temperatures near the freezing point, although $NaCl(H_2O)_5$ is certainly supported by our analysis. However, the claim (Max and Chapados 2001) that $NaCl(H_2O)_5$ is present at all concentrations is neither proved nor disproved by this study since our data mostly relate to concentrated solutions. We can only say that the existence of $NaCl(H_2O)_5$ in highly concentrated solutions (saturated and/or near freezing) is supported by this finite cluster analysis. The existence of $NaCl(H_2O)_{10}$ and other similar clusters is probable when the solution has insufficient water molecules to fully solvate Na^+ and Cl^- as independent aqueous ions.

Conclusions

Freezing sea water concentrates the salts and frost flowers can act as wicks to expose high concentrations of salts to reactions in the lower atmosphere. Our most important conclusion is that we find support for the

finite cluster $NaCl(H_2O)_5$ postulated in previous study by others (Max and Chapados 2001), which is likely to be found in concentrated, cold brines. However, other finite clusters such as $NaCl(H_2O)_{10}$ are probably present as well as $NaCl(H_2O)_5$ at whatever freezing point that is operative. The structure found here for $NaCl(H_2O)_{10}$ is also compatible with earlier molecular dynamic modeling (Jungwirth and Tobias 2001) in which it was found that Cl^- tends to be preferentially brought to the surface of aqueous salt solutions. Such behavior enables the formation of gaseous, reactive species such as BrCl. Note that our spectrum of 0.1 M NaCl at +1.7 °C shown in Fig. 2 is shifted less to the blue of the ice spectrum than colder films, which is consistent with decreasing amounts of $NaCl(H_2O)_5$ and other water-deficient species like $NaCl(H_2O)_{10}$ as more water is available. It should be noted that we have extended the concept of finite cluster analysis to the liquid state. The resonating hydrogen bonds in $NaCl(H_2O)_5$ are a strong feature of the vibrational spectrum of that species, and it is likely that it contributes to the observed blue shift in the spectrum of NaCl brine at temperatures near the melting point. Other studies of inclusions in solid ice or minerals containing Na^+ ions may invoke solid-state models, but the focus of this study is on the liquid brine near the freezing point of a NaCl solution.

Acknowledgments The authors wish to thank Mr. Mike Davis on the staff of Academic Computing at Virginia Commonwealth University for installing the Actos V4.6 operating system and the GAMESS program on our computer. The experimental study was funded in part by a Chenery Research Fellowship (RMC), and R.W. was supported by the Schapiro Undergraduate Research Fellowship (RMC).

References

Alvarez-Aviles L, Simpson WR, Douglas TA, Sturm M, Perovich D, Domine F (2008) Frost flower chemical composition during growth and its implications for aerosol production and bromine activation. J Geophys Res 113: D21304. doi:10.1029/2008JD010277

Barrow GM (1988) Physical chemistry, 5th edn. McGraw-Hill Book Co, New York, p 308

Becke AD (1988) Density-functional exchange-energy approximation with correct asymptotic behavior. Phys Rev A 38: 3098–3100

Becke AD (1993a) A new mixing of Hartree–Fock and local density-functional theories. J Chem Phys 98:1372–1377

Becke AD (1993b) Density-functional thermochemistry. III. The role of exact exchange. J Chem Phys 98:5648–5652

Becke AD (1996) Density-functional thermochemistry. IV. A new dynamical correlation functional and implications for exact-exchange mixing. J Chem Phys 104:1040–1046

Binkley JS, Pople JA (1975) Moeller-Plesset theory for atomic ground state energies. Int J Quantum Chem IX:229–236

Bode BM, Gordon MS (1998) MacMolPlt: a graphical user interface for GAMESS. J Mol Graphics Mod 16:133–138

Callahan MP, Crews B, Abo-Rizig A, Grace L, de Vries MS, Gengeliczki Z, Holmes TM, Hall GA (2007) IR-UV double resonance spectroscopy of xanthine. Phys Chem Chem Phys 9:4587–4591

Davidson ER, Morokuma K (1984) A proposed anti-ferroelectric structure for proton ordered ice 1 h. J Chem Phys 81:3741–3742

Debye P, Hückel E (1923) Zur Theorie der Elektrolyte. I. Gefrierpunktserniedrigung und verwandte Erscheinungen [The theory of electrolytes. I. Lowering of freezing point and related phenomena]. Physikalische Zeitschrift **24:**185–206; on-line @ http://electrochem.cwru.edu/estir/hist/hist-12-Debye-1.pdf

Douglas TA, Sturm M, Simpson WR, Brooks S, Lindberg SE, Perovich DK (2005) Elevated mercury measured in snow and frost flowers near Arctic sea ice leads. Geophys Res Lett 32:L04502. doi:10.1029/2004GL022132

Eisenberg D, Kauzmann W (1969) The structure and properties of water. Oxford University Press, Oxford

Esperdy K, Shillady DD (2001) Simulated infrared spectra of Ho(III) and Gd(III) chlorides and carboxylates using effective core potentials in GAMESS. J Chem Inf Comput Sci 41:1547–1552

Foresman JB, Frisch A (1996) Exploring chemistry with electronic structure methods, 2nd edn. Gaussian Inc, Pittsburg, p 64

Foster KL, Plastridge RA, Bottenheim JW, Shepson PB, Finlayson-Pitts BJ, Spicer CW (2001) The role of Br2 and BrCl in surface ozone at polar sunrise. Science 291: 471–474

Gordon MS, Schmidt MW (2005) Advances in electronic structure theory: GAMESS a decade later (Chapter 41). In: Dykstra CE, Frenking G, Kim KS, Scuseria GE (eds) Theory and applications of computational chemistry, the first forty years. Elsevier, Amsterdam, pp 1167–1189

Haynes WH (ed) (2012) Concentrative properties of aqueous solutions: density, refractive index, freezing point depression, and viscosity. In: CRC Handbook of chemistry and physics, 92nd edn, Internet Version, CRC Press/Taylor and Francis, Boca Raton

Hogness TR, Johnson WC (1954) Ionic equilibrium as applied to qualitative analysis, 3rd edn. Henry Holt and Co, New York

Jungwirth P, Tobias DJ (2001) Molecular structure of salt solutions: a new view of the interface with implications for heterogeneous atmospheric chemistry. J Phys Chem B 105:10468–10472

Lee C, Yang W, Parr RG (1988) Development of the Colle-Salvetti correlation-energy formula into a functional of the electron density. Phys Rev B 37:785–789

Lu JY, Schroeder WH, Barrie LA, Steffen A (2001) Magnification of atmospheric mercury deposition to polar regions in springtime: the link to tropospheric ozone depletion chemistry. Geophys Res Lett 28:3219–3222

Max JJ, Chapados C (1999) Interpolation and extrapolation of infrared spectra of binary ionic aqueous solutions. Appl Spectrosc 53:1601–1609

Max JJ, Chapados C (2001) IR spectroscopy of aqueous alkali halide solutions: pure salt-solvated water spectra and hydration numbers. J Chem Phys 115:2664–2675

Max JJ, deBlois S, Veilleux A, Chapados C (2001) IR Spectroscopy of aqueous alkali halides. Factor analysis. Can J Chem 79:13–21

Roothaan CCJ (1951) New developments in molecular orbital theory. Rev Mod Phys 23:69–89

Scott AP, Radom L (1996) Harmonic vibrational frequencies: an evaluation of Hartree-Fock, Møller-Plesset, quadratic configuration interaction, density functional theory, and semiempirical scale factors. J Phys Chem 100:16502–16513

Shillady DD, Nguyen TT, Jena P (1982) Calculation of the ground state energy of hydrogen at interstitial sites in a lithium cluster. In: Satterthwaite C, Jena P (eds) Electronic structure and properties of hydrogen in metals. Plenum, NY, pp 291–295

Su MD, Liao HY, Chung WS, Chu SY (1999) Cycloadditions of 16-electron 1,3-dipoles with ethylene. A density functional and CCSD(T) study. J Org Chem 64:6710–6716

Zhao Y, Truhlar DG (2005) Benchmark databases for nonbonded interactions and their use to test density functional theory. J Chem Theory Comput 1:415–432